

# Shape and Reflectance from RGB-D Images using Time Sequential Illumination

Matis Hudon<sup>1,2</sup>, Adrien Gruson<sup>1</sup>, Paul Kerbiriou<sup>2</sup>, Remi Cozot<sup>1</sup> and Kadi Bouatouch<sup>1</sup>

<sup>1</sup>*IRISA, Rennes 1 University, Rennes, France*

<sup>2</sup>*Technicolor, Rennes, France*

{mhudon, agruson, rcozot, kadi}@irisa.fr; paul.kerbiriou@technicolor.com

**Keywords:** Depth Enhancement, Depth Discontinuity, Time Multiplexed Illumination, Image Pairs, Pure Flash Image.

**Abstract:** In this paper we propose a method for recovering the shape (geometry) and the diffuse reflectance from an image (or video) using a hybrid setup consisting of a depth sensor (Kinect), a consumer camera and a partially controlled illumination (using a flash). The objective is to show how combining RGB-D acquisition with a sequential illumination is useful for shape and reflectance recovery. A pair of two images are captured: one non flashed (image under ambient illumination) and a flashed one. A pure flash image is computed by subtracting the non flashed image from the flashed image. We propose an novel and near real-time algorithm, based on a local illumination model of our flash and the pure flash image, to enhance geometry (from the noisy depth map) and recover reflectance information.

## 1 INTRODUCTION

Low-cost RGB-Depth scanners have recently led to a little revolution in computer graphics and computer vision areas with many direct applications in robotics, motion capture and scene analysis. The main concern of such depth sensors is their low accuracy due to noise and their inherent quantization (see raw depth image in Figure 1). The idea of improving depth using the information contained in the associated RGB image has been widely explored (Diebel and Thrun, 2005; Richardt et al., 2012; Nehab et al., 2005; Wu et al., 2014). It relies on building a complete model of the scene by estimating and ideally extracting separately materials, 3D shape and illumination. The depth sensor usually provides a rough estimate of the scene geometry which is then refined using lighting and materials (extracted from RGB images) as well as shape from shading-based algorithms.

On the other hand, stereo photometry methods have been used for years to extract finer geometry and materials from images of a scene (Woodham, 1980; Kim et al., 2010; Debevec, 2012). Unfortunately, the use of stereo photometry is inappropriate in most of the shooting scenarios as it requires finer calibration and a complex lighting setup. Therefore stereo photometry methods cannot be easily incorporated into a traditional movie framework.

In our new technique, we explore the possibilities

given by a hybrid setup consisting of a depth sensor together with a partially controlled illumination. We target a low-cost and the least intrusive possible setup. Our idea is to use RGB flashed and non-flashed image pairs. To obtain such pairs we perform a time sequential illumination by triggering flash illuminations on half the frames of the RGB camera and then extracting two sequences of the same scene: one corresponding to the scene with its natural illumination and no alterations, preserving then the shooting framework, and another containing flashed images.

With a proper combination of the two images of an image pair, we create a pure flash image, as if the unknown ambient illumination had been switched off, which amounts to take a picture of the scene under the flash illumination only (DiCarlo et al., 2001). This provides us with a sequence of images with a controlled and simple illumination, which simplifies the ill-posed problem of retrieving separately shapes and albedos from a single image. We use raw depth input to estimate a rough normal map, and our knowledge of the flash illumination to reconstruct high quality normals and albedos for each pixel using a simple iterative mean square optimization. The main contributions of this paper are:

- a new method, to efficiently recover geometry and albedo from image sequences, using a hybrid setup combining sequential illumination and consumer depth sensors;

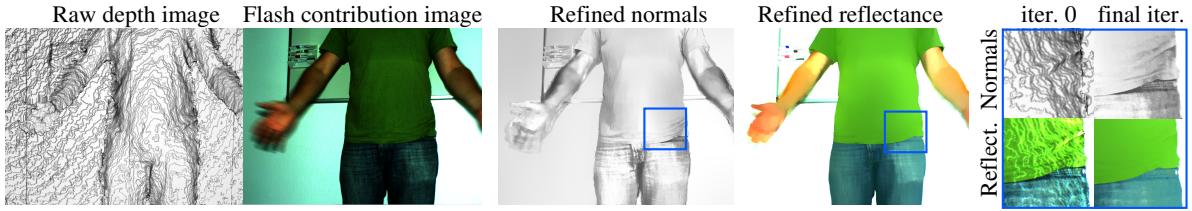


Figure 1: Our method takes as input a flash image registered with a depth map (Kinect). The flash image is computed using flashed and non flashed image pairs which represent two successive video frames. With these inputs our algorithm use an optimization process to produce refined normal and reflectance maps.

- robustness to multiple albedo scenes;
- near real-time performance.

## 2 RELATED WORK

**Shape from Shading.** (Horn, 1970) Introduced the shape from shading technique, using intensity patterns across an image, under the assumption of Lambertian reflectance and uniform illumination, to extract 3D geometry. Later (Horn and Brooks, 1989) explored variational approaches to shape from shading. (Bruckstein, 1988) derived fine height maps from scenes illuminated from above, using a shape from shading method based on a recursive way of determining equal-height contours. More recently (Prados and Faugeras, 2005; Fanello et al., 2014) used controlled light sources near the camera optical center and took into account the inverse squared distance attenuation term of the illumination in a shape from shading approach.

**Depth Upsampling.** (Diebel and Thrun, 2005) used Markov Random Fields to fuse data from a low resolution depth scanner and a high resolution color camera. (Richardt et al., 2012) proposed an efficient and effective depth filtering and upsampling techniques for RGB-D videos, but take no advantage of shading in their framework. Their heuristic approach look plausible but may not be metrically accurate. (Nehab et al., 2005) devised an efficient algorithm for combining depths and normals while taking advantage of each to create the best geometry possible for computer graphics purposes. (Wu et al., 2014) presented a real-time method to solve the inverse rendering problem using an effective parametrization of the shading equation. Their method allows refining a depth map captured by consumer depth camera for lambertian scenes with a time varying uncontrolled illumination. Recently (Or-El et al., 2015) proposed a novel method to enhance the depth captured with low-cost RGB-D scanners without the need to explicitly find and integrate surface normals. Their method gives accurate results and runs in real-time, it achieves

10 fps for  $640 \times 480$  depth profiles. We provide more details on this technique in the result section as we compare it to our method. (Newcombe et al., 2015) presented an impressive SLAM method capable of reconstructing non-rigid deforming scenes in real-time, by fusing RGBD scans captured from commodity sensors.

**Intrinsic Image Decomposition.** (Shen et al., 2008) described the possibility of separating, in a single image, shading from reflectance by relying on the observation that distinct points with the same intensity-normalized texture configuration generally have the same reflectance value. (Shen and Yeo, 2011) based on chromaticity to show that the reflectance in a natural image is sparse. Using this sparsity prior they formulated a regularized least square minimization problem that can be solved efficiently, their algorithm successfully extract an intrinsic image from a single image.

**Photometric Stereo** was firstly introduced by (Woodham, 1980). (Higo et al., 2010) pushed the photometric stereo a little further replacing the lambertian prior by three reflectance properties: monotonicity, visibility and isotropy. This allows to capture more surfaces including specular ones, but the system requires many pictures with different directions of illumination. (Tunwattanapong et al., 2013) presented a way for acquiring geometry and spatially varying reflectance properties using spherical harmonic illuminations. They developed a system comprising a rotating arm capable of reproducing spherical harmonic illumination. Photometric stereo works very well for fixed scenes but as it requires at least three observations of the scene under different and non co-planar illuminations, it is by nature difficult to use for video. Several attempts have been made to adapt photometric stereo to video. Indeed, (Kim et al., 2010) and (Hernández et al., 2007) use colored lights to obtain several images (with different lighting directions) in a single snapshot. (de Decker et al., 2009) used both colored lights and time multiplexed images to perform photometric stereo (with more than 3 light directions) on video sequences. This method resolves low frame rate issues inherent in photometric stereo

applied to video, but suffers from some issues. For example, the method fails when the spectra of one of the light sources and the albedo of an object do not overlap. (Wenger et al., 2005) proposed a method to acquire live-action performance of an actor, allowing lighting and reflectance to be designed and modified in post-production. They obtained excellent results but need a highly controlled environment and a synchronization device between lights and cameras. (Debevec, 2012) presented a variety of facial scanning and reflectance measurements works achieved with light stage system. They obtained results that are very impressive but cannot be incorporated in many traditional shooting scenarios as they require a complex lighting and synchronization setup.

**Image Pairs.** After the report of (Xiao et al., 2001), that showed that, using active light sources, it is possible to measure object information independently of the passive illuminant. (DiCarlo et al., 2001) had the idea of combining two images, one with ambient unknown illumination and the other with an additional controlled and known illumination, to obtain an image without ambient illumination and then estimate the spectral power distribution of the ambient illumination. More recently (Petschnigg et al., 2004) used pairs of flashed and non flashed images for various applications in digital photography, including denoising, detail transfer, white balancing and red-eye removal.

### 3 GENERAL IDEA

Under the assumption of Lambertian scene a photometric stereo-based method uses three observations (three images) of the same scene, under different illuminations, to compute surface normals and diffuse reflectances (albedo). Now imagine a single albedo scene illuminated by a single known light source. It is possible to estimate a rough normal map with a low-cost RGB-D sensor, and so for each point in the scene it is easy to compute the diffuse reflectance from the shading equation and the rough normal map. As the measured normals are not perfectly estimated the diffuse reflectance computed for each point is different rather than similar (errors on normal estimation affect the diffuse reflectance estimation), but the scene is supposed to be a single albedo scene, which means that all the diffuse reflectances have to be equal. If we suppose that the errors on normal estimation are equally distributed over the range of possible normal directions, a single albedo of the scene can be estimated by averaging all the obtained diffuse reflectances. We now have an estimate of the scene dif-

fuse reflectance together with a knowledge of the only light source within the scene. The normal map estimate can then be improved using the shading equation. Those new computed normals can be used as input for a novel per-point estimation of diffuse reflectance. This process can be repeated until convergence.

For natural scenes, we relax the assumption of single albedo to consider multiple albedos by assuming that the reflectance of these scenes is sparse (Shen and Yeo, 2011). Using chromaticity, we can cluster points in the scene so that each cluster contains points of nearly the same diffuse reflectance. As for illumination, we use pairs of flashed and non flashed images to extract pure flash images (DiCarlo et al., 2001).

**Light Source Modeling.** We assume that the flash LED light source is small, consequently the light source will be characterized by its intensity  $I_s$ :

$$I_s(\omega_i) = L_s \cdot \Delta S \cdot |N(S) \cdot \omega_i| \quad (1)$$

where  $\Delta S$  is the surface area of the flash light source,  $L_s$  its emitted luminance,  $N(S)$  its normal and  $\omega_i$  its emission direction. With this assumption, we can easily compute the reflected luminance  $L$  of an point  $P$  as seen through a pixel in direction  $\omega_c$  as:

$$L(P, \omega_c) = fr(P, \omega_i \rightarrow \omega_c) \cdot I_s(\omega_i) \cdot \frac{|N(P) \cdot \omega_i|}{\|P - S\|^2} \quad (2)$$

where  $fr$  is the bidirectional reflectance distribution function (BRDF) of the surface,  $\omega_i$  the emission direction of the light source,  $N(P)$  the surface normal at  $P$  and  $\|P - S\|$  the distance between the flash light source and  $P$ .

**Scene Illumination.** Let  $p$  be a pixel of coordinates  $(u, v)$  on the camera sensor (centered coordinates). This pixel can be projected onto the scene as a 3D point  $P(u, v)$  expressed in the camera coordinate system by using the camera parameters:

$$P(u, v) = \begin{pmatrix} u \cdot \mathcal{D}(u, v) / f_x \\ v \cdot \mathcal{D}(u, v) / f_y \\ -\mathcal{D}(u, v) \end{pmatrix} \quad (3)$$

where  $(f_x, f_y)$  are the camera focals and  $\mathcal{D}(u, v)$  is the depth value given by the depth sensor expressed in the  $rgb$  camera coordinate system. For a Lambertian surface, the luminance of a point  $P$  can be expressed as:

$$L(P(u, v), \omega_c) = k_d(u, v) \cdot I_s(\omega_i) \cdot \frac{|N(u, v) \cdot \omega_i|}{d^2} \quad (4)$$

where  $d = \|P - S\|$ . The diffuse reflectances  $k_d$  (for each color component RGB) and the surface normals  $N$  are stored into two different 2D buffers. From now on, we will use  $p = (u, v)$  and  $L(P(u, v), \omega_c) = L(p)$  for each RGB component  $c$ .

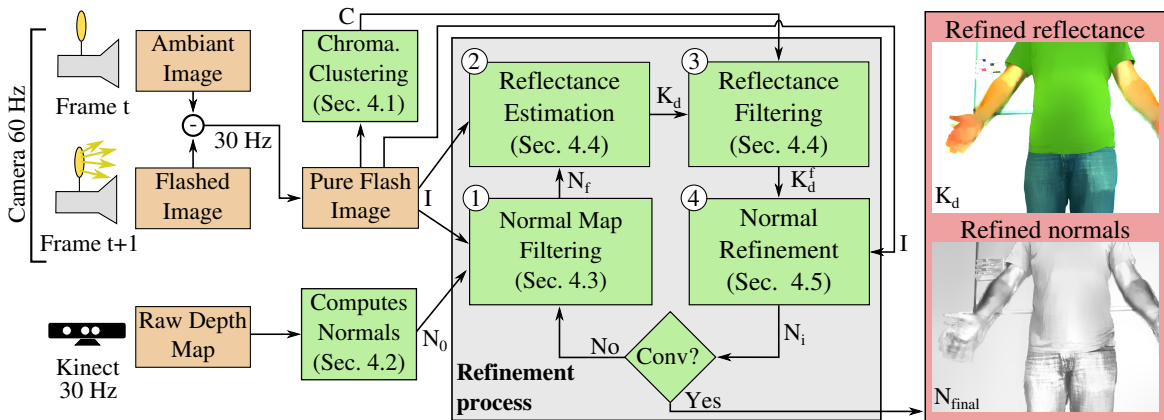


Figure 2: Our framework picture. Green boxes represent the different processings of our algorithm. Orange boxes represent the values given by the sensors at different times. Red box is the result of our algorithm.

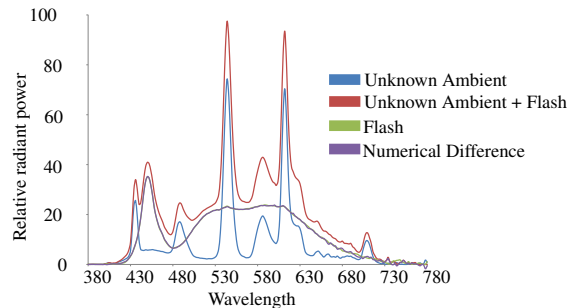


Figure 3: Blue: Spectrum of a white Lambertian point under the unknown ambient illumination. Red: Spectrum of a white Lambertian point under unknown ambient illumination and flash illumination (total spectrum). Green: Spectrum of a white Lambertian point under pure flash illumination. Purple: difference between the total spectrum and the ambient spectrum, this difference spectrum completely matches the pure flash spectrum.

**Pure Flash Image from Image Pairs.** Our goal is to create a pure flash image from a pair of two images: a flashed and non-flashed one (also called ambient image). As we record our images with a time sequential illumination we use the same aperture and exposure time for the two images. The flashed image can be recovered by subtracting the ambient image from the flashed one, provided that the images are linear and do not contain any underexposed and saturated pixels. As shown in Figure 3, to validate this subtraction (to compute the pure flash image) we have captured a white Lambertian point under several illuminations with a spectrometer and subtracted the spectrum of the ambient illumination from the total spectrum (obtained after triggering the flash). This results in a spectrum that matches the spectrum obtained with a pure flash illumination. To make sure that the combination of the two images of a pair provides a pure flash image, three caveats should be considered: (1) the two

images must be taken with the same camera parameters (exposure time, aperture, focal length), (2) the images have to be linear, (3) the pixels color should not be saturated nor underexposed in the two images. Moreover, as a luminous power decreases with the inverse squared distance, objects too far away might not receive enough light energy from the flash illumination. This restrains the scenario setup to scenes not too far from the camera.

## 4 OUR APPROACH

Our approach is summarized in Figure 2. First, our hybrid setup (a camera, a Kinect and a Flash) is completely calibrated to register the Kinect depth image to the RGB camera. The illumination of the scene is known (pure flash image) thanks to our time sequential illumination. Moreover, as we also know the extrinsic and intrinsics parameters of our setup, we can project the depth map (provided by the Kinect) onto a 3D point map in the camera coordinate system. Before refining the normal and the reflectance maps, we compute a rough normal map from the raw depth map provided by the Kinect (Section 4.2). Then we use the pure flash image to cluster (K-means clustering) the 3D points seen through the pixels camera, each cluster containing points of nearly the same diffuse reflectance (Section 4.1). Then we start our iterative refinement process consisting of 4 steps. In the first step (Section 4.3), we filter the normal map, the weights being depended on luminance to preserve geometry details and coherence. The second step (Section 4.4) performs an estimation of a reflectance map from the pure flashed image and the filtered normal map. In third step (Section 4.4), a filter is applied to the reflectance map with weights depending on chroma

maticity. During the last step (Section 4.5), the normal map is refined thanks to a shading least square minimization that allows to fit our model to the pure flash image. Finally, we repeat those steps until convergence, say when both the normal and reflectance maps do not vary anymore. Now, we will detail the different steps in the following subsections. For convenience purpose, as the images and the depths are registered, from now on, a point is either a pixel  $p$  of an image captured by the camera or the 3D point  $P$  seen through  $p$ .

## 4.1 Chromaticity Assumption

As in (DiCarlo et al., 2001), we suppose that the chromaticity of the scene is sparse. This assumption allows us to perform a color segmentation of the scene based on quadratic chromaticity distance. The segmentation consists in applying a K-means clustering to the input image so that each pixel is assigned a cluster of a given chromaticity (Figure 4). Each pixel is projected onto a 3D point with a diffuse reflectance. Each cluster is supposed to contain pixels of nearly the same diffuse reflectance. We initialize the K-means centers (10 in our current implementation) by spreading them in the chromaticity gamut. More robust clustering techniques are left for future work.

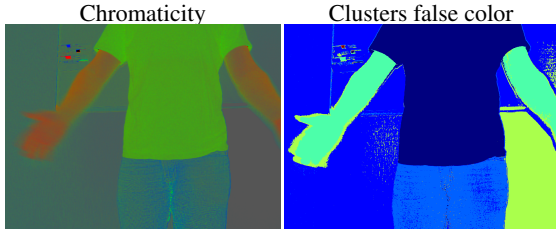


Figure 4: The chromaticity image is used to cluster surfaces with similar diffuse reflectances. We can observe that the t-shirt, the background and the skin are classified into different clusters.

## 4.2 Computing Normal Map from Quantified Depth Data

Let us use the raw depth map (captured by the Kinect) to compute  $N(p)$ , the normal associated with a pixel  $p$ . To compute this normal, we need to express the depth changes  $(\delta_x(u, v), \delta_y(u, v))$  as follows:

$$\delta_x(u, v) = \mathcal{D}(u+1, v) - \mathcal{D}(u-1, v) \quad (5)$$

$$\delta_y(u, v) = \mathcal{D}(u, v+1) - \mathcal{D}(u, v-1) \quad (6)$$

The normal, associated with the pixel  $p$ , can be estimated as:

$$T_x(p) = \left( 2 \cdot \frac{\mathcal{D}(p)}{f_x} \quad 0 \quad -\delta_x(p) \right)^T \quad (7)$$

$$T_y(p) = \left( 0 \quad 2 \cdot \frac{\mathcal{D}(p)}{f_y} \quad -\delta_y(p) \right)^T \quad (8)$$

$$N(p) = T_x(p) \times T_y(p) \quad (9)$$

where  $T_x(p)$  and  $T_y(p)$  are respectively the tangents to the surface according to the  $X$  and  $Y$  axes respectively. Note that, as the Kinect depth map is quantized, it represents a piece-wise constant approximation of the real depth map (see Figure 1). Due to this quantization artifact, most of the normals, computed from this depth map, will be oriented toward the camera, which is a poor initial guess for our normal map refinement algorithm. This quantization artifact makes the normal map noisy. Consequently, to overcome the quantization artifact and other possible artifacts, an important part of our algorithm consists in filtering the normal map. This filtering is detailed in the next subsection.

## 4.3 Normal Map Filtering

To remove noise in the normal map, we apply a bilateral filter to the normals  $N$  (computed from the depth map) to get filtered normals  $N_f$ :

$$N_f(p) = \frac{1}{W_n(p)} \sum_{s \in \Omega(p)} \Psi_N(s, p) N(s) \quad (10)$$

where  $W_n(p)$  is a normalization factor,  $\Omega(p)$  a neighborhood of the pixel  $p$  and  $\Psi_N$  the weighting function. The expression of the weighting function depends on the luminance  $L$  of the pixels of the pure flash image and on the normals:

$$\Psi_N(s, p) = \exp \left( -\frac{(L(p)-L(s))^2}{2\sigma_l^2} - \frac{\|N(p)-N(s)\|^2}{2\sigma_n^2} \right)$$

where  $\sigma_l$  and  $\sigma_n$  are weighting parameters related to luminance and normal respectively. Numerical values used in our experiments are given in the results section. The reason of adding the luminance information in the weighting function is to preserve geometry details, as the luminance value changes locally with the normal orientation.

## 4.4 Reflectance Estimation and Filtering

Let us consider the case of Lambertian surfaces. The RGB pixel values of  $p$  captured by the camera can be estimated as follows:

$$I(p) = \frac{I_s(\omega_i)}{d^2} \cdot k_d(p) \cdot |N(p) \cdot \omega_i| \quad (11)$$

$I_s$ ,  $d$ ,  $\omega_i$  are known as the source illumination is controlled,  $k_d(p)$  is the diffuse reflectance of a Lambertian surface.  $k_d$  is commonly expressed for each  $\{r,g,b\}$  component. Refining the normal map requires an estimation of those diffuse reflectances.

Once the first rough estimation of the normals has been performed, Equation 2 is used to estimate the reflectance map:

$$k_d(p) = \frac{d^2}{I_s(\omega_i)} \cdot \frac{I(p)}{|N(p) \cdot \omega_i|}, \quad (12)$$

where  $I(p)$  is the  $\{r,g,b\}$  value of a pixel of the pure flash image and  $I_s$  the intensity of the flash light source. The reflectance map is rough as it is computed from a rough depth map. However, the pure flash image can help improve the reflectance map, provided that the two following assumptions are satisfied:

1. if two points have the same normal, the difference between their pixel values is only due to albedo change,
2. the distribution of reflectance over the image is sparse to ensure a reliable segmentation (Section 4.1).

According to the two above assumptions, any albedo change is due to chromaticity change (DiCarlo et al., 2001), in other words any chromaticity change entails an albedo change. Consequently, the impact of normal aberration, on the reflectance map, can be reduced by averaging the diffuse reflectances of points lying in a neighborhood. This averaging operation is performed using another bilateral filter:

$$k_d^f(p) = \frac{1}{W_d(p)} \sum_{s \in \Omega(p)} \Psi_d(s, p) k_d(s) \quad (13)$$

where  $W_d(p)$  is the normalization factor,  $\Psi_d$  being the weighting function which depends on chromaticity similarities. Indeed, if two points are not assigned the same chromaticity cluster (Section 4.1), their weights are set to zero. The condition that two pixels  $p$  and  $s$  belong to the same cluster is:

$$C(s, p) = (C(s) = C(p)) \text{ and } (|m(s) - m(p)| < t_m)$$

where  $C(p)$  is the cluster id associated with pixel  $p$ ,  $m(p)$  is the maximum of the  $r, g, b$  values of the pixel  $p$  and  $t_m$  a threshold value that we set to 0.5. The second term is added to make the distinction between black and white points. Finally, the expression of the weight used in Equation 13 is given by:

$$\Psi_d(s, p) = \begin{cases} \exp\left(\frac{-\|m(s) - m(p)\|^2}{2\sigma_m^2}\right) & \text{if } C(s, p) \\ 0 & \text{otherwise} \end{cases}$$

where  $\sigma_m$  is a weighting parameter. Numerical values used in our experiments are given in the results section. To avoid that black, white and grey pixels mingle during the filtering process, we use a weight which depends on the maximum  $m$  of the  $r, g, b$  values of each pixel.

## 4.5 Normal Map Refinement

Once the reflectance map filtered, the next step consists in refining the normal map. Our refinement relies on the lambertian model and a least-square error like algorithm for the three channels of each pixel. Equation 4 can be written as:

$$I(p) = \frac{I_s(\omega_i) \cdot k_d(p)}{d^2} \cdot (N_x \omega_x + N_y \omega_y + N_z \omega_z) \quad (14)$$

Let us assume that the right  $k_d$  reflectances are available, the goal is to find the three components of normal  $N$  that minimize  $\xi$  over the set of the three  $rgb$  components:

$$\xi(p) = \left( \sum_c (S(p, c) - (N_x \omega_x + N_y \omega_y + N_z \omega_z))^2 \right)^2$$

$$S(p, c) = \frac{I(p, c) \cdot d^2}{k_d(p, c) \cdot I_s(\omega_i)}$$

where  $k_d(p, c)$  and  $I(p, c)$  are respectively the diffuse reflectance and the value of pixel  $p$  for the color channel  $c$ . We want to find the minimum error with respect to  $(N_x, N_y, N_z)$ , which is reached when:

$$\frac{\partial \xi}{\partial N_x}(p) = 0 \rightarrow N_x = \frac{\sum_c (S(p, c) - N_z \omega_z - N_y \omega_y)}{3 \cdot \omega_x^2}$$

$$\frac{\partial \xi}{\partial N_y}(p) = 0 \rightarrow N_y = \frac{\sum_c (S(p, c) - N_x \omega_x - N_z \omega_z)}{3 \cdot \omega_y^2}$$

$$\frac{\partial \xi}{\partial N_z}(p) = 0 \rightarrow N_z = \frac{\sum_c (S(p, c) - N_x \omega_x - N_y \omega_y)}{3 \cdot \omega_z^2}$$

In the minimization process, each normal  $N = (N_x \ N_y \ N_z)^T$  is initialized with the rough normal map computed from he Kinect depth data, then each component of the normals is computed through an iterative scheme until convergence.

## 4.6 Global Convergence

The plots on Figure 5 illustrate the convergence of the Normal Map and the diffuse reflectance map when applying our iterative algorithm. We computed the mean distance between the normal map (respectively the diffuse reflectance map) evaluated at the current iteration and the normal map (respectively the diffuse reflectance map) evaluated at the preceding iteration.

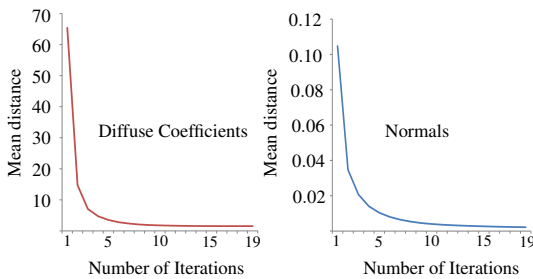


Figure 5: Plots representing the convergence of Normals and Diffuse Reflectances for each iteration.

Figure 5 demonstrates that only a few iterations are necessary to reach a steady state. Indeed, only 4 – 5 iterations are necessary to reach a high quality Normal and reflectance maps.

## 5 RESULTS

Our experimental setup consists of: a Kinect depth sensor (depth res.  $640 \times 480$ , frame rate 30 fps), a Ueye Industrial Camera (res.  $1280 \times 960$ , frame rate 60 fps with a global shutter) and a flash LED light. An electronic board is used to synchronize the camera with the flash. This allows to sequentially acquire an image pair: flashed and non flashed. So, we are able to generate an image pair at 30 fps. The Kinect is not synchronized due to its own limitations. The depth image is upsampled to match the camera resolution.

We have implemented our technique in C++ and used CUDA 6.5 to speedup all the steps of our algorithm. The details of the algorithm timings are summarized in Table 1. All the timings in this table have been measured on an a Xeon ES 2640 CPU  $2.5\text{GHz} \times 2$  (32GB Ram) and an Nvidia Geforce GTX 580. Note that the image registration step is not included into our timings. Indeed, its performance depends on the setup and the chosen technique. For example, in (Or-El et al., 2015), this operation takes 31.1 ms per frame on an Nvidia Titan GPU. The algorithm parameters were set to:  $\sigma_m = 0.002$ ,  $\sigma_l = 0.0004$  and  $\sigma_n = 0.02$ , these values were carried throughout all experiments. For the two filtering operations (normal and reflectance maps), we use a kernel of 20 pixels size except for the **Burger scene** (Figure 6) for which we use a kernel of 10 pixels size. This is due to the fact that the image of this scene is twice smaller than that of the other test scenes (Figure 1 and 8).

Our method is compared to (Or-El et al., 2015). To this end, we used the Matlab code provided by the authors. Their method aims at enhancing a depth map by fusing intensity and depth information to cre-

Table 1: Timings of each step of our algorithm. **Bold** timings are obtained using the performance improvement described in the next subsection. To compute the total time, we need to multiply the refinement iteration time by the number of iterations needed to converge to the desired results. In practice, only 5 iterations are required, which corresponds to 5.84 fps or 0.23 fps on a GTX 580 using or not using the performance improvement. Note that the "Image Alignment" step timing is taken from (Or-El et al., 2015).

Operations		Time (ms)
Init.	Image Alignment*	31.1
	Chroma Clustering	7.34
	3D Points Estim.	0.24
Refine iter.	Normal Filtering	495.55 <b>(0.43)</b>
	Dot Calculation	0.70
	Reflectance Estim.	0.26
	Reflectance Filtering	345.74 <b>(17.39)</b>
	Normal Refinement	7.72
	Total Refinement Iteration	849.97 <b>(26.5)</b>
	Total Time (5 iterations)	4288.53 <b>(171.18)</b>

ate detailed range profiles. For this purpose, they use a lighting model that can handle natural illumination. This model is integrated in a shape-from-shading technique to improve the reconstruction of objects. Note that, unlike our method, their approach refines the depths rather than the normals.

Figure 6 shows a comparison between our method and the one of (Or-El et al., 2015) for a synthetic **Burger scene**. The input depth map is perturbed by adding a gaussian white noise. To use our algorithm, we rendered the scene using a small light source that simulates the flash. Our method produces results with an error smaller than the one obtained with the method of (Or-El et al., 2015). This is particularly visible on the tomatoes where fine details are well recovered. However, there is more noise on the bread due to clustering issues (Figure 7).

The scene (Figure 8), is a real scene with relatively slow arm movements. Unlike the method of (Or-El et al., 2015) no mask is used to select the main object. The input depth map is noisy as it is directly provided by the Kinect sensor. This noise is different from the synthetic one used in Figure 6. Compared to (Or-El et al., 2015), our method provides results that have less artifacts and fine geometry details are correctly recovered. The main issue of (Or-El et al., 2015) method is the use of a bilateral filter which is applied to filter a lot of data due to the high level of noise in the raw depth map. Our two filtering operations are performed using bilateral filters. But, as we use them at each iteration, a smaller kernel size is needed, which reduces the artifacts inherent in large kernel bilateral filters. Furthermore, at each iteration we compute new normals (Normal Refine-

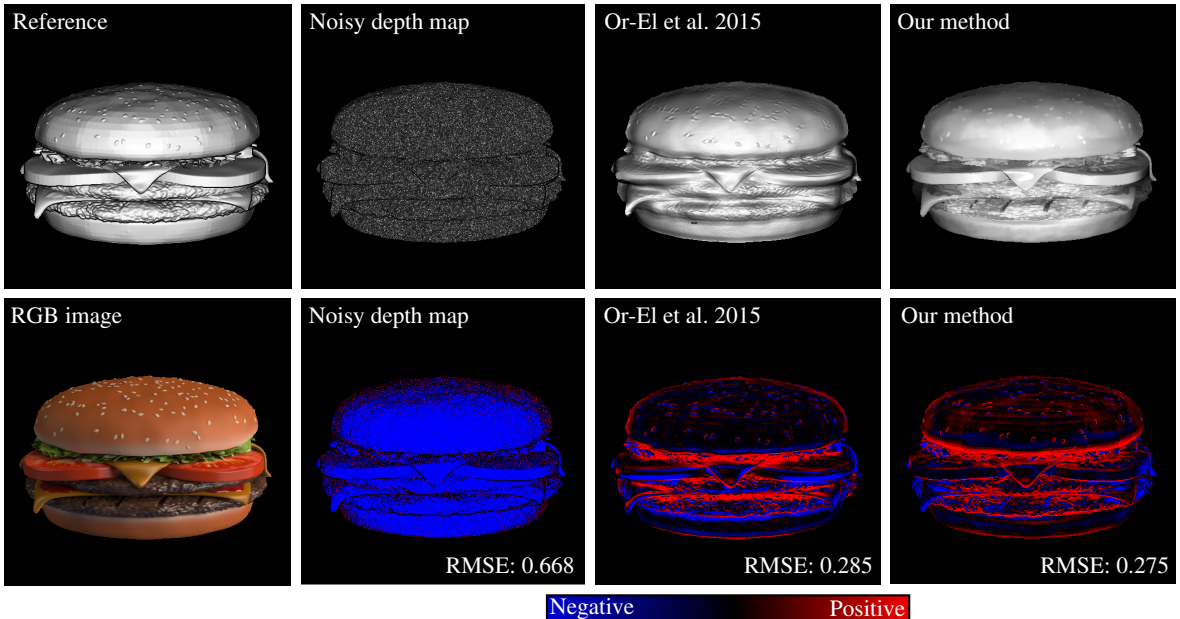


Figure 6: The original burger scene used in (Or-El et al., 2015). Top row show the dot product image (dot product between the normal and the view direction) using the normals of: the reference solution, the noisy map used as input, (Or-El et al., 2015) and our method. Bottom row show the RGB image and the false color error on the normal dot product. For better visualisation the error was multiplied by 3.

ment operation) and new reflectances (Reflectance Estimation operation). Consequently, artifacts due to successive bilateral filtering operations are avoided.

**Performance Improvement.** One of the bottleneck of our algorithm is the two filtering operations (Normal Filtering and Reflectance Filtering) which take 495.553 ms and 345.74 ms respectively. These two operations use non separable filters, which are time consuming. However, to reduce the computing time, those filters can be approximated by separable filters with weights carefully computed. The error due to those approximations are hardly visible. The computing times needed by the separable version of these two filters are 0.49 ms ( $1005 \times$  faster) and 17.39 ms ( $20 \times$  faster). All the timings are summarized in Table 1. Except for the **Burger scene**, due to the reduced image size, this optimization has been used for all the scenes (Figures 1 and 8). Better and more robust optimization is left for future work.

**Application.** One direct application of our algorithm is the relighting of a captured scene. Indeed, our algorithm provides the reflectance and the normal maps of a scene that we relight with artificial light sources (Figure 9). In this scene, the movement of the arms is fast. This explains the artifacts on the arms due to motion blur.

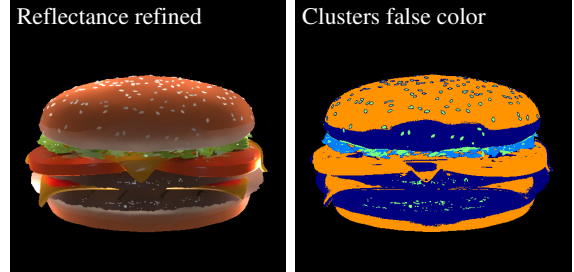


Figure 7: On the left: the refined reflectance map after convergence of our algorithm. On the right: false color image to show how the chromaticity-based clustering performs. We can observe that the tomatoes and the bread lie in the same cluster. However, due to the local nature of the filtering, these two material have not been merged.

## 6 CONCLUSIONS

We showed that even with a consumer camera and a Kinect (capturing noisy depth data) it is possible to recover finer geometry and precise diffuse reflectances from an image or a video thanks to the use of sequential illumination provided by a flash. A pair of two images are captured: one non flashed image (image under ambient illumination) and a flashed one. A pure flash image is computed by subtracting the non flashed image from the flashed image. We proposed an efficient iterative algorithm to recover shapes and

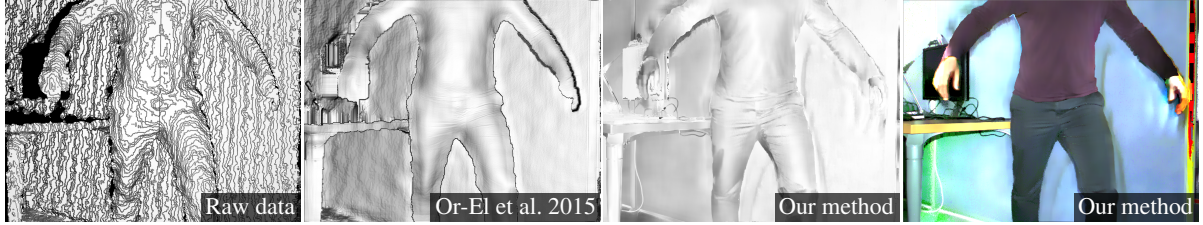


Figure 8: T-Shirt scene captured by our setup. From left to right: The raw data display using the dot product, (Or-El et al., 2015) using the dot product, our method with the dot product and the reflectance map.



Figure 9: The normal and reflectance maps refined by our algorithm can be used for relighting a scene. Images Relighting 1 & 2 are obtained with different artificial light source positions. Moreover, sequential lighting makes our technique capable of capturing video sequences. However, fast and large movements in the video could create artifacts due to motion blur.

reflectances from the pure flash image. The fact of knowing the illumination (flash light source) makes the extraction of normals and reflectances easier and more efficient. Indeed, as the position and the photometry of the flash light source is known, we used a local illumination model to express the normal and the diffuse reflectance for each pixel. From the computed normals we used the illumination equations to determine the reflectances. In turn, these reflectances are fed to a process that determines new normals. This process is repeated until convergence. We showed that only a few iterations are needed to converge to the desired results.

## REFERENCES

- Bruckstein, A. M. (1988). On shape from shading. *Computer Vision, Graphics, and Image Processing*, 44(2):139–154.
- de Decker, B., Kautz, J., Mertens, T., and Bekaert, P. (2009). Capturing multiple illumination conditions using time and color multiplexing. In *2009 IEEE Computer Society Conference on Computer Vision and Pattern Recognition (CVPR 2009)*, 20-25 June 2009, Miami, Florida, USA, pages 2536–2543.
- Debevec, P. (2012). The light stages and their applications to photoreal digital actors. *SIGGRAPH Asia Technical Briefs*.
- DiCarlo, J. M., Xiao, F., and Wandell, B. A. (2001). Illuminating illumination. In *Color and Imaging Conference*, volume 2001, pages 27–34. Society for Imaging Science and Technology.
- Diebel, J. and Thrun, S. (2005). An application of markov random fields to range sensing. In *Advances in neural information processing systems*, pages 291–298.
- Fanello, S. R., Keskin, C., Izadi, S., Kohli, P., Kim, D., Sweeney, D., Criminisi, A., Shotton, J., Kang, S. B., and Paek, T. (2014). Learning to be a depth camera for close-range human capture and interaction. *ACM Transactions on Graphics (TOG)*, 33(4):86.
- Hernández, C., Vogiatzis, G., Brostow, G. J., Stenger, B., and Cipolla, R. (2007). Non-rigid photometric stereo with colored lights. In *ICCV*.
- Higo, T., Matsushita, Y., and Ikeuchi, K. (2010). Consensus photometric stereo. In *Computer Vision and Pattern Recognition (CVPR), 2010 IEEE Conference on*, pages 1157–1164. IEEE.
- Horn, B. K. (1970). Shape from shading: A method for obtaining the shape of a smooth opaque object from one view.
- Horn, B. K. and Brooks, M. J. (1989). *Shape from shading*. MIT press.
- Kim, H., Wilburn, B., and Ben-Ezra, M. (2010). Photometric stereo for dynamic surface orientations. In *Computer Vision - ECCV 2010, 11th European Conference on Computer Vision, Heraklion, Crete, Greece, September 5-11, 2010, Proceedings, Part I*, pages 59–72.
- Nehab, D., Rusinkiewicz, S., Davis, J., and Ramamoorthi, R. (2005). Efficiently combining positions and normals for precise 3d geometry. *ACM transactions on graphics (TOG)*, 24(3):536–543.
- Newcombe, R. A., Fox, D., and Seitz, S. M. (2015). Dynamicfusion: Reconstruction and tracking of non-rigid scenes in real-time. In *Proceedings of the IEEE Conference on Computer Vision and Pattern Recognition*, pages 343–352.
- Or-El, R., Rosman, G., Wetzler, A., Kimmel, R., and Bruckstein, A. M. (2015). Rgbdfusion: Real-time high precision depth recovery. In *Proceedings of the IEEE Conference on Computer Vision and Pattern Recognition*, pages 5407–5416.
- Petschnigg, G., Szeliski, R., Agrawala, M., Cohen, M., Hoppe, H., and Toyama, K. (2004). Digital photography with flash and no-flash image pairs. *ACM transactions on graphics (TOG)*, 23(3):664–672.
- Prados, E. and Faugeras, O. (2005). Shape from shading: a well-posed problem? In *Computer Vision and Pattern*

- Recognition, 2005. CVPR 2005. IEEE Computer Society Conference on*, volume 2, pages 870–877. IEEE.
- Richardt, C., Stoll, C., Dodgson, N. A., Seidel, H.-P., and Theobalt, C. (2012). Coherent spatiotemporal filtering, upsampling and rendering of rgbz videos. In *Computer Graphics Forum*, volume 31, pages 247–256. Wiley Online Library.
- Shen, L., Tan, P., and Lin, S. (2008). Intrinsic image decomposition with non-local texture cues. In *Computer Vision and Pattern Recognition, 2008. CVPR 2008. IEEE Conference on*, pages 1–7. IEEE.
- Shen, L. and Yeo, C. (2011). Intrinsic images decomposition using a local and global sparse representation of reflectance. In *Computer Vision and Pattern Recognition (CVPR), 2011 IEEE Conference on*, pages 697–704. IEEE.
- Tunwattanapong, B., Fyffe, G., Graham, P., Busch, J., Yu, X., Ghosh, A., and Debevec, P. (2013). Acquiring reflectance and shape from continuous spherical harmonic illumination. *ACM Transactions on graphics (TOG)*, 32(4):109.
- Wenger, A., Gardner, A., Tchou, C., Unger, J., Hawkins, T., and Debevec, P. (2005). Performance relighting and reflectance transformation with time-multiplexed illumination. 24(3):756–764.
- Woodham, R. J. (1980). Photometric method for determining surface orientation from multiple images. *Optical Engineering*, 19(1):191139–191139–.
- Wu, C., Zollhöfer, M., Nießner, M., Stamminger, M., Izadi, S., and Theobalt, C. (2014). Real-time shading-based refinement for consumer depth cameras. *Proc. SIGGRAPH Asia*.
- Xiao, F., DiCarlo, J. M., Catrysse, P. B., and Wandell, B. A. (2001). Image analysis using modulated light sources. In *Photonics West 2001-Electronic Imaging*, pages 22–30. International Society for Optics and Photonics.